Published in final edited form as:

J Am Chem Soc. 2022 July 27; 144(29): 13055–13059. doi:10.1021/jacs.2c05491.

Enzyme Responsive Rigid-Rod Aromatics Target "Undruggable" Phosphatases to Kill Cancer Cells in Mimetic Bone Microenvironment

Meihui Yi[1], **Fengbin Wang**[2], **Weiyi Tan**[1], **Jer-Tsong Hsieh**[3], **Edward H. Egelman**[2], **Bing Xu**[1]

[1]Department of Chemistry, Brandeis University, 415 South Street, Waltham, MA 02453, USA

[2]Department of Biochemistry and Molecular Genetics, University of Virginia, Charlottesville, VA 22908, USA

[3]Department of Urology, Southwestern Medical Center, University of Texas, Dallas, TX 75235, USA

Abstract

Bone metastasis remains a challenge in cancer treatment. Here we show that enzymatic responsive rigid-rod aromatics, acting as the substrates of "undruggable" phosphatases, to kill cancer cells in mimetic bone microenvironment. By phosphorylation and conjugating nitrobenzoxadiazole (NBD) to hydroxybiphenylcarboxylate (BP), we obtained pBP-NBD (**1P**) as a substrate of both acid and alkaline phosphatases. **1P** effectively kill both metastatic castration-resistant prostate cancer cells (mCRPCs) and osteoblast mimic cells in their co-culture. **1P** enter Saos2 almost instantly to target the endoplasmic reticulum (ER) of the cells. Co-culturing with Saos2 cells boosts the cellular uptake of **1P** by mCRPCs. Cryo-EM reveals the nanotube structures of both **1P** (2.4 Å resolution, pH 5.6) and **1** (2.2 Å resolution, pH 7.4). The helical packing of both nanotubes is identical, held together by strong pi-stackings interactions. Besides reporting the atomistic structure of nanotubes formed by the assembly of rigid-rod aromatics, this work expands the pool of molecules for designing EISA substrates that selectively target TME.

Graphical Abstract

Corresponding Author: **Bing Xu** − Department of Chemistry, Brandeis University, 415 South Street, Waltham, MA 02453, USA; bxu@brandeis.edu, **Edward Egelman**- Department of Biochemistry and Molecular Genetics, University of Virginia, Charlottesville, VA 22908, USA; egelman@virginia.edu. **Jer-Tsong Hsieh**- Department of Urology, Southwestern Medical Center, University of Texas, Dallas, TX 75235, USA; JT.Hsieh@utsouthwestern.edu.

Supporting Information

Materials and detailed experimental procedures, TEM and CLSM images, cell viabilities, chemical structures of the compounds (PDF), and coordinates of the cryo-EM structures (PDB).

The authors declare no competing financial interests.

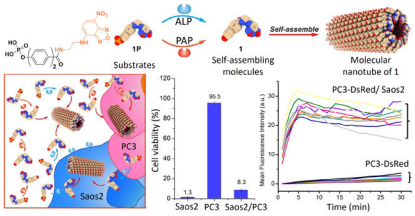

This communication reports the first example of enzyme-instructed self-assembly (EISA) of rigid-rod aromatics for killing cancer cells in mimetic bone microenvironment. Despite considerable progress in cancer therapy, tumor metastasis still causes most of cancer-related death.[1] For example, approximately 90% of patients who die of prostate cancer have bone metastases.[2] Bone metastases are a vicious self-reinforcing cycle in tumor microenvironment (TME), where cancer cells promote the differentiation of osteoclasts and osteoblasts, and the increased bone turnover releases cytokines to benefit metastatic cancer cells. Moreover, bone is also a site for further spread of other metastasis.[3] The current treatment of bone metastasis, Radium-223 (Ra-223)[4,5] is only palliative because the acceptable radiation dosage of Radium-223 is limited. Thus, there is an urgent need to develop novel approaches for killing cancer cells in bone metastasis sites or TME with minimal side effects. Inspired by the dual targeting mode-of-action of Radium-223, we are aiming to develop non-radioactive small molecules as a single agent that self-assemble in-situ or on-site to kill both metastatic castration-resistant prostate cancer (mCRPC) and osteoblast cells in TME.

A prominent feature of osteoblastic mCRPC at the TME is that mCRPC and osteoblasts overexpress prostatic acid phosphatase (PAP)[6] and alkaline phosphatase (ALP)[7], respectively. However, developing inhibitors of PAP and ALP to treat mCRPC has been unsuccessful for several reasons: (i) PAP acts as tumor suppressor,[8] (ii) inhibitor of ALP is unable to inhibit cancer cells,[9] and (iii) most phosphatases previously are considered as undruggable targets.[10–11] Thus, we decide to explore EISA, which kills cancer cells by enzymatic reaction and self-assembly,[12] for developing therapeutics for osteoblastic mCRPC. EISA is particularly attractive because EISA kills cancer cells without inhibiting the targeted enzymes. Moreover, ALP is metabolically inert in serum,[13] a subtlety allowing EISA to occur at TME. Recently, a variety of small molecule substrates, including peptides,[14–18] carbohydrates,[19] and lipids,[20–21] of ALP-based EISA are able to induce death of the cancer cells that overexpressing ALP because EISA allows “on-site” generating nanostructures from small molecules.[22] Although peptide-based substrates are the most explored among these building blocks up-to-date, their efficacy for killing mCRPC still remains to be improved.[23] Thus, we choose to examine other nonpeptidic molecules as the self-assembling building blocks for EISA against mCRPC.

Based on aggregate advisors[24] and rigid-rod molecules for self-assembly, we choose a rigid-rod aromatic molecule, biphenyl, as the core motif for developing EISA substrates of PAP and ALP. Biphenyl has found various applications in liquid crystals,[25–28] dendrimers,[29] long-range self-assembly,[30] amphiphiles,[31] peptides.[32] We recently found that biphenyl enable rapid enzymatic self-assembly and hydrogelation of peptides.[33] But biphenyl has yet to be explored for EISA without involving peptides. Based on the above rationale, we

phosphorylated the hydroxyl and conjugated a fluorophore (nitrobenzoxadiazole (NBD)) at the carboxylic end of hydroxybiphenylcarboxylate (BP) or hydroxyterphenylcarboxylate (TP) to produce pBP-NBD (**1P**) or pTP-NBD (**2P**), respectively. As a substrate of both PAP and ALP, **1P** effectively kills both metastatic castration-resistant prostate cancer cells (mCRPCs) (VCaP or PC3) and osteoblast mimic cells (Saos2) in their co-culture. Fluorescent imaging shows that **1P** enters Saos2 almost instantly to target the endoplasmic reticulum (ER) of the cells and that Saos2 in the co-culture boosts the cellular uptake of **1P** or **2P** by VCaP or PC3 cells. Cryo-EM reveals that the **1** (from dephosphorylating **1P** at physiological pH) or **1P** (at acidic pH) self-assembles to form cones with C7 symmetry, and the supramolecular cones stack helically with a 3.5 Å rise to form nanotubes. Besides reporting the atomistic structure of nanotubes formed by the assembly of rigid-rod aromatics, this work, using enzymatic reactions to form intracellular nanotubes of small rigid-rod molecules, expands the pool of molecules for designing EISA substrates that selectively target TME.

Scheme 1 shows the structures and the key synthetic step for making, **1P**, **2P**, and **3P**, which have biphenyl, terphenyl, and phenyl motifs, respectively. While BP and hydroxylphenylcarboxylate are commercially available, TP is produced in almost quantitative yield from 4-bromo-4’-hydroxylbiphenyl and 4-carboxyphenylboronic acid by palladium-catalyzed cross coupling.[34] Mixing BP or hydroxylphenylcarboxylate with phosphorus pentachloride directly under heat or reacting TP with phosphorous oxychloride in pyridine produces the phosphorylated aromatic carboxylic acids. After getting all three phosphorylated compounds, we conjugated them with NBD-ethylene diamine to generate **1P**, **2P,** and **3P**.

As shown by transmission electron microscopy (TEM), adding ALP to solution of **1P** (500 μM and pH7.4) transforms the amorphous aggregates of **1P** to ~7 nm diameter nanotubes of **1** (Figure 1). At pH 5.6, **1P** (50 μM) forms nanotubes like those of **1.** These results indicate **1P** self-assembling more readily at lower pH because protonation decreases phosphate repulsion. Adding PAP in **1P** solution (50 μM and at pH 5.6) results in more nanotubes (Figure 1). Adding ALP to the solution of **2P** also switches the aggregates of **2P** into nanotubes with similar diameters (Figure S2). At pH 5.6, **2P** (50 μM) transforms from aggregates into twisted nanoribbons (Figure S1). **3P** exists as amorphous aggregates both at pH 7.4 or pH 5.6 and rarely forms nanotubes after adding ALP or PAP (Figure S1), indicating that noncovalent interactions from phenyl are insufficient for **3P** or **3** to self-assemble into nanotubes.

We tested **1P** for its activity against six different cell lines, Saos2, SJSA1, VCaP, PC3, HepG2 and PNT1A (Figures 2A and S4). **1P** shows the first day IC_{50} around 20.9 μM against Saos2 cells. The IC_{50} values of **1P** against SJSA1 and Saos2 are comparable, except day 1. While **1P** significantly inhibit VCaP and PC3 cells from day 2 and day 3, respectively, **1P** is rather compatible with HepG2 and PNT1A even at day 3, with IC_{50} around 108 μM and 89 μM. Even though **2P** showed potent activity against Saos2 and SJSA1, it hardly inhibits VCaP, PC3, HepG2 and PNT1A (Figures S3 and S4). Compared to **1P** and **2P**, **1** and **2** is more toxic to the normal prostate cells, PNT1A, indicating

that phosphorylation enhances the selectivity for targeting cancer cells. ALP inhibitor (DQB) reduces the cytotoxicity of **1P** and **2P** against Saos2 or SJSA1 cells (Figure S5), indicating that ALP-catalyzed EISA of **1P** and **2P** contributes to their cytotoxicity. The low cytotoxicity of **1P** and **2P** towards hepatocyte (HepG2) indicates low toxicity of **1P** and **2P** to liver. **3P** hardly inhibits these cells (Figure S2B), consistent with the poor self-assembling ability of **3**. M-β-CD, an inhibitor for caveolae mediated endocytosis, rescues Saso2 and SJSA1 treated by **1P** or **2P**, suggesting that **1P** or **2P** enters the cells via endocytosis (Figure S6).

As shown in Figure 2B, 1P enters Saos2 or SJSA1 within 1 minute and accumulates inside the cells. On the other hand, **1P** accumulates in VCaP or PC3 cells slowly that visible fluorescence from **1** emerges in VCaP and PC3 cells after 30 and 60 minutes, respectively. The inhibitory activity of **1P** correlates well with the rate of cellular uptake, except in the case of HepG2. Although **1P** enters HepG2 faster (Figure S7) than entering PC3, **1P** hardly inhibits HepG2, agreeing with detoxification function of hepatocytes.[35] **2P** exhibits a similar trend as that of **1P** to enter Saos2, SJSA1, VCaP, and PC3 cells (Figure S9). Agreeing with its cell compatibility, **3P** enters Saos2 much slower than **1P** or **2P** does (Figure S8).

For Saos2 and SJSA1 cells, the distribution of **1P** in cytosol resembles to that of ER (Figures 2C and S10). Co-staining **1P** with ER-tracker, Lyso-tracker, or Mito-tracker in Saos2 or SJSA1 cells shows that the fluorescence from **1P** mostly overlaps with the fluorescence of ER-tracker, indicating that **1P**, after entering cells and being dephosphorylated, specifically localizes in ER of Saos2 and SJSA1. The ER accumulation agrees with that phosphobipenyl is a substrate of PTP1B[36], which mainly locates at ER[37]. **2P** localizes more in ER of Saos2 and SJSA1 cells than in lysosomes and mitochondria, and forms denser fluorescent puncta in Saos2 and SJSA1 than **1P** does (Figures S11 and S12). The fluorescence of **1P** in VCaP and PC3 cells overlap more with that of Lysotracker, indicating that **1P** mainly undergoes dephosphorylation in the lysosomes. This result agrees with that PAP localized in lysosome.[38]

We cocultured the mCRPC cells (e.g., VCaP or PC3) and the osteoblast mimic cells (Saos2) in a 1:1 ratio to create a mimetic bone microenvironment and tested the efficacy of **1P**. As shown in Figure 3A, being incubated with **1P** for 24 h, the viability of Saos2 or VCaP cells is 1.6% and 41.3%, respectively. The cell viability of the coculture of Saos2 and VCaP is 1.9% after adding **1P** in the coculture. Similarly, **2P** inhibits VCaP more effectively in the coculture. Moreover, Figure 3B shows the viability of PC3 cells, being incubated with **1P** or **2P** in the co-culture of PC3 and Saos2, is significantly lower than that of PC3 cells alone. These results suggest that Saos2 in the coculture significantly enhances the inhibitory activity of **1P** or **2P** against VCaP or PC3 cells. Fluorescence imaging reveals the cellular uptake of **1P** by VCaP or PC3 cells (Figures 3C, D, S13–15). The fluorescence in the VCaP or PC3 cells increases faster in the coculture than being cultured alone. These results indicate that Saos2 cells, in the co-culture, boost the cellular uptake of **1P** or **2P** by VCaP and PC3 cells, thus leading to more effective inhibition of VCaP or PC3 cells.

We used cryo-EM and determined the high-resolution nanotube structures of both **1** at pH 7.4 and **1P** at pH 5.6 (Figures S16A and S17A). Possible helical symmetries were calculated

from the averaged power spectrum of boxed filaments (Figures S16B and S17B) and the correct ones were found[39]. The nanotubes of **1** and **1P** have almost identical diameters (Figure 4A–B) and helical symmetries (Figure 4C–D, Table S1), with aromatic rings held together by extensive pi-stacking interactions (Figure 4E). The NBD motifs points to the center and the biphenyl groups constitute the periphery of the nanotubes. The ability of **1P** to form nanotubes at pH 5.6 is consistent with the lysosomal accumulation of **1P** (Figure 2A, C) and its increased activities against VCaP and PC3 cells after 48 h.

In summary, this work reports a new class of EISA substrates to form nanotubes for effectively killing osteoblast model cells and mCRPCs in mimetic bone TME. The toxicity of **1** and **2** to PNT1A imply that nanotubes of 1 or 2 likely results in cell death. It illustrates the dual targeting mode-of-action of EISA substrates, which promising to kill both cancer and osteoblast cells at bone TME. Although the detailed mechanism of action of EISA of **1P** or **2P** in the co-culture remains to be elucidated, using the enzymatic feature of TME to boost cellular uptake of EISA substrates in mCRPCs promising a new way to target TME of mCRPCs. The approach reported here should be applicable to other aggregation-prone small molecules or drug candidates,[24, 40] which may lead to more effective EISA substrates for targeting TME of other metastatic cancers.

Supplementary Material

Refer to Web version on PubMed Central for supplementary material.

ACKNOWLEDGMENT

This work is partially supported by NIH CA142746 (B.X.) and CA252364 (B.X.), GM122510 (E.H.E.), K99GM138756 (F.W.) and NSF DMR-2011846 (B.X.).

REFERENCES

1. American Cancer Society. Cancer Facts & Figures 2022. Atlanta: American Cancer Society; 2022.
2. Pego ER; Fernández I; Núñez MJ, Molecular basis of the effect of MMP-9 on the prostate bone metastasis: A review. Urol. Oncol. Semin. Orig. Invest 2018, 36 (6), 272–282.
3. Zhang W; Bado IL; Hu J; Wan YW; Wu L; Wang H; Gao Y; Jeong HH; Xu Z; Hao X; Lege BM; Al-Ouran R; Li L; Li J; Yu L; Singh S; Lo HC; Niu M; Liu J; Jiang W; Li Y; Wong STC; Cheng C; Liu Z; Zhang XH, The bone microenvironment invigorates metastatic seeds for further dissemination. Cell 2021, 184 (9), 2471–2486 e20. [PubMed: 33878291]
4. Cha TL; Wu TTL; Vogelzang NJ; Huang CY; Huang SP; Lin CC; Ou YC; Pang ST; Shen DHY; Wu WJ; Chang WYH, Optimal usage of radium-223 in metastatic castration-resistant prostate cancer. J. Formos. Med. Assoc 2017, 116 (11), 825–836. [PubMed: 29046247]
5. Suominen MI; Fagerlund KM; Rissanen JP; Konkol YM; Morko JP; Peng Z; Alhoniemi EJ; Laine SK; Corey E; Mumberg D; Ziegelbauer K; Käkönen SM; Halleen JM; Vessella RL; Scholz A, Radium-223 inhibits osseous prostate cancer growth by dual targeting of cancer cells and bone microenvironment in mouse models. Clin. Cancer Res 2017, 23 (15), 4335–4346. [PubMed: 28364014]
6. Kirschenbaum A; Liu XH; Yao S; Leiter A; Levine AC, Prostatic acid phosphatase is expressed in human prostate cancer bone metastases and promotes osteoblast differentiation. In Ann Ny Acad Sci, Blackwell Publishing Inc.: 2011; Vol. 1237, pp 64–70. [PubMed: 22082367]
7. Heinrich D; Bruland O; Guise TA; Suzuki H; Sartor O, Alkaline phosphatase in metastatic castration-resistant prostate cancer: Reassessment of an older biomarker. Future Oncology 2018, 14 (24), 2543–2556. [PubMed: 29925281]

8. Lin M-F; Lee M-S; Zhou X-W; Andressen JC; Meng T-C; Johansson SL; West WW; Taylor RJ; Anderson JR; Lin F-F, Decreased Expression of Cellular Prostatic Acid Phosphatase Increases Tumorigenicity of Human Prostate Cancer Cells. Journal of Urology 2001, 166 (5), 1943–1950. [PubMed: 11586265]
9. Wang H; Feng Z; Wang Y; Zhou R; Yang Z; Xu B, Integrating Enzymatic Self-Assembly and Mitochondria Targeting for Selectively Killing Cancer Cells without Acquired Drug Resistance. J Am Chem Soc 2016, 138 (49), 16046–16055. [PubMed: 27960313]
10. Stanford SM; Bottini N, Targeting Tyrosine Phosphatases: Time to End the Stigma. Trends Pharmacol Sci 2017, 38 (6), 524–540. [PubMed: 28412041]
11. Vainonen JP; Momeny M; Westermarck J, Druggable cancer phosphatases. Sci. Trans. Med 2021, 13 (588), eabe2967.
12. He H; Tan W; Guo J; Yi M; Shy AN; Xu B, Enzymatic Noncovalent Synthesis. Chem Rev 2020, 120 (18), 9994–10078. [PubMed: 32812754]
13. Kaplan MM, Alkaline phosphatase. N Engl J Med 1972, 286 (4), 200–2. [PubMed: 4550137]
14. Yang ZM; Xu KM; Guo ZF; Guo ZH; Xu B, Intracellular Enzymatic Formation of Nanofibers Results in Hydrogelation and Regulated Cell Death. Adv. Mater 2007, 19 (20), 3152–3156.
15. Kuang Y; Shi J; Li J; Yuan D; Alberti KA; Xu Q; Xu B, Pericellular hydrogel/nanonets inhibit cancer cells. Angew Chem Int Ed Engl 2014, 53 (31), 8104–7. [PubMed: 24820524]
16. Tanaka A; Fukuoka Y; Morimoto Y; Honjo T; Koda D; Goto M; Maruyama T, Cancer cell death induced by the intracellular self-assembly of an enzyme-responsive supramolecular gelator. J Am Chem Soc 2015, 137 (2), 770–5. [PubMed: 25521540]
17. Zhou J; Du X; Yamagata N; Xu B, Enzyme-Instructed Self-Assembly of Small D-Peptides as a Multiple-Step Process for Selectively Killing Cancer Cells. J Am Chem Soc 2016, 138 (11), 3813–23. [PubMed: 26966844]
18. Gao Y; Kuang Y; Guo ZF; Guo Z; Krauss IJ; Xu B, Enzyme-instructed molecular self-assembly confers nanofibers and a supramolecular hydrogel of taxol derivative. J Am Chem Soc 2009, 131 (38), 13576–7. [PubMed: 19731909]
19. Pires RA; Abul-Haija YM; Costa DS; Novoa-Carballal R; Reis RL; Ulijn RV; Pashkuleva I, Controlling cancer cell fate using localized biocatalytic self-assembly of an aromatic carbohydrate amphiphile. J Am Chem Soc 2015, 137 (2), 576–9. [PubMed: 25539667]
20. Wang H; Feng Z; Wu D; Fritzsching KJ; Rigney M; Zhou J; Jiang Y; Schmidt-Rohr K; Xu B, Enzyme-Regulated Supramolecular Assemblies of Cholesterol Conjugates against Drug-Resistant Ovarian Cancer Cells. J Am Chem Soc 2016, 138 (34), 10758–61. [PubMed: 27529637]
21. Wang J; Tan W; Li G; Wu D; He H; Xu J; Yi M; Zhang Y; Aghvami SA; Fraden S; Xu B, Enzymatic Insertion of Lipids Increases Membrane Tension for Inhibiting Drug Resistant Cancer Cells. Chemistry 2020, 26 (66), 15116–15120. [PubMed: 32579262]
22. Parak WJ; Weil T; Weiss PS, A Virtual Issue on Nanomedicine. ACS Nano 2021, 15 (10), 15397–15401.
23. Feng Z; Wang H; Yi M; Lo CY; Sallee A; Hsieh JT; Xu B, Instructed-Assembly of Small Peptides Inhibits Drug-Resistant Prostate Cancer Cells. Pept Sci (Hoboken) 2020, 112 (1), e24123.
24. Irwin JJ; Duan D; Torosyan H; Doak AK; Ziebart KT; Sterling T; Tumanian G; Shoichet BK, An Aggregation Advisor for Ligand Discovery. J Med Chem 2015, 58 (17), 7076–87. [PubMed: 26295373]
25. Durbin SD; Arakelian SM; Shen YR, Optical-field-induced birefringence and Freedericksz transition in a nematic liquid crystal. Physical Review Letters 1981, 47 (19), 1411–1414.
26. Kouwer PHJ; Swager TM, Synthesis and mesomorphic properties of rigid-core ionic liquid crystals. J. Am. Chem. Soc 2007, 129 (45), 14042–14052. [PubMed: 17949091]
27. Kato T; Hirota N; Fujishima A; Fréchet JMJ, Supramolecular hydrogen-bonded liquid-crystalline polymer complexes. Design of side-chain polymers and a host-guest system by noncovalent interaction. J Polym Sci Part A 1996, 34 (1), 57–62.
28. Cao Y; Alaasar M; Zhang L; Zhu C; Tschierske C; Liu F, Supramolecular meso-Trick: Ambidextrous Mirror Symmetry Breaking in a Liquid Crystalline Network with Tetragonal Symmetry. J Am Chem Soc 2022, 144 (15), 6936–6945. [PubMed: 35394276]

29. Peterca M; Imam MR; Leowanawat P; Rosen BM; Wilson DA; Wilson CJ; Zeng X; Ungar G; Heiney PA; Percec V, Self-assembly of hybrid dendrons into doubly segregated supramolecular polyhedral columns and vesicles. J. Am. Chem. Soc 2010, 132 (32), 11288–11305. [PubMed: 20698696]
30. Van Esch J; De Feyter S; Kellogg RM; De Schryver F; Feringa BL, Self-assembly of bisurea compounds in organic solvents and on solid substrates. CHEM. EUR. J 1997, 3 (8), 1238–1243.
31. Kunitake T; Okahata Y; Shimomura M; Yasunami SI; Takarabe K, Formation of Stable Bilayer Assemblies in Water from Single-Chain Amphiphiles. Relationship between the Amphiphile Structure and the Aggregate Morphology. J. Am. Chem. Soc 1981, 103 (18), 5401–5413.
32. Nesloney CL; Kelly JW, A 2,3'-substituted biphenyl-based amino acid facilitates the formation of a monomeric β-hairpin-like structure in aqueous solution at elevated temperature. J. Am. Chem. Soc 1996, 118 (25), 5836–5845.
33. Yi M; Guo J; He H; Tan W; Harmon N; Ghebreyessus K; Xu B, Phosphobisaromatic motifs enable rapid enzymatic self-assembly and hydrogelation of short peptides. Soft Matter 2021, 17, 8590–8594. [PubMed: 34545895]
34. Jansa J; Řezníček T; Jambor R; Bureš F; Lyčka A, Synthesis of Hydroxy-Substituted p-Terphenyls and some Larger Oligophenylenes via Palladium on Charcoal Catalyzed Suzuki-Miyaura Reaction. Advanced Synthesis & Catalysis 2017, 359 (2), 339–350.
35. Miners JO; Knights KM; Houston JB; Mackenzie PI, In vitro–in vivo correlation for drugs and other compounds eliminated by glucuronidation in humans: Pitfalls and promises. Biochemical Pharmacology 2006, 71 (11), 1531–1539. [PubMed: 16455060]
36. Montserat J; Chen L; Lawrence DS; Zhang ZY, Potent low molecular weight substrates for protein-tyrosine phosphatase. J Biol Chem 1996, 271 (13), 7868–7872. [PubMed: 8631832]
37. Haj FG; Verveer PJ; Squire A; Neel BG; Bastiaens PIH, Imaging Sites of Receptor Dephosphorylation by PTP1B on the Surface of the Endoplasmic Reticulum. Science 2002, 295 (5560), 1708–1711. [PubMed: 11872838]
38. Tappel A, Lysosomal and prostasomal hydrolytic enzymes and redox processes and initiation of prostate cancer. Medical Hypotheses 2005, 64 (6), 1170–1172. [PubMed: 15823710]
39. Wang F; Gnewou O; Solemanifar A; Conticello VP; Egelman EH, Cryo-EM of Helical Polymers. Chem Rev 2022. DOI: 10.1021/acs.chemrev.1c00753
40. McGovern SL; Caselli E; Grigorieff N; Shoichet BK, A common mechanism underlying promiscuous inhibitors from virtual and high-throughput screening. J Med Chem 2002, 45 (8), 1712–22. [PubMed: 11931626]

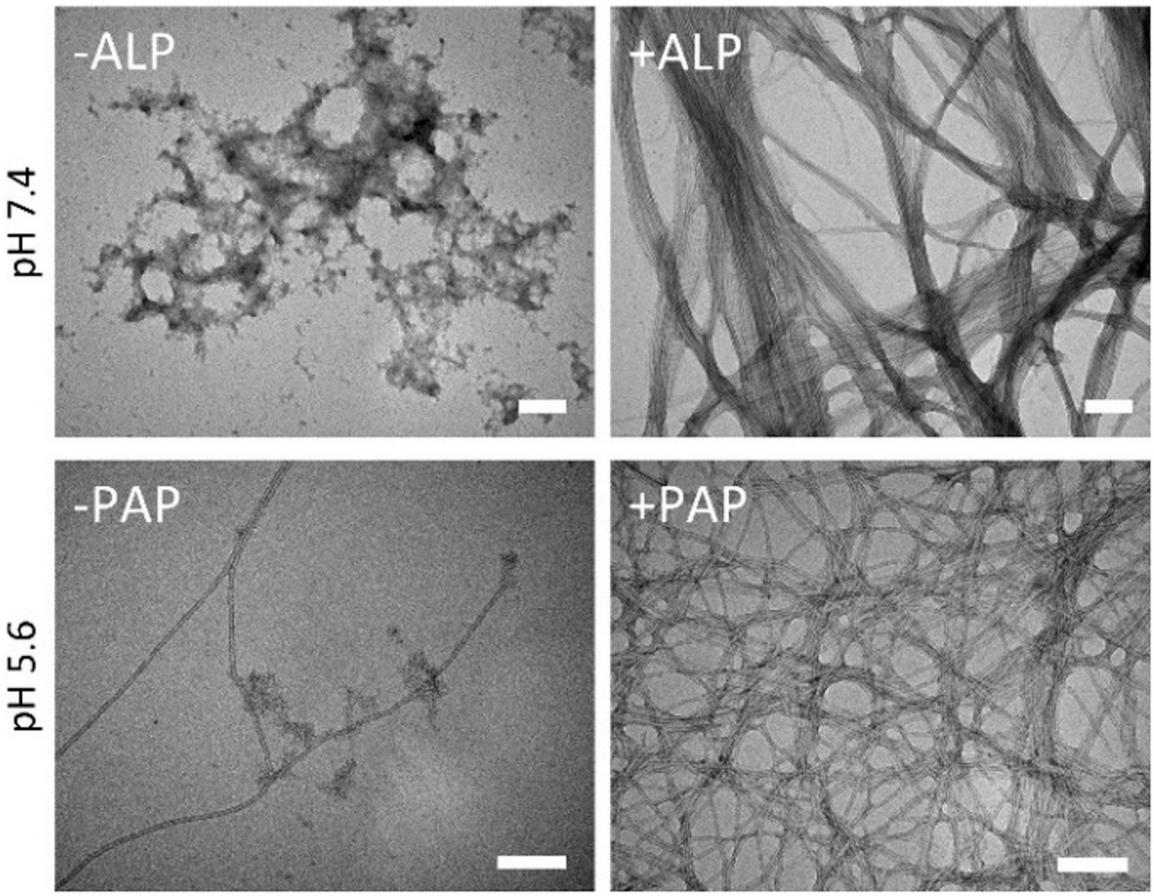

Figure 1.

TEM of **1P** (500 μM, pH 7.4) before and after adding ALP (0.1 U/mL) for 24 h and of **1P** (50 μM, pH 5.6) before and after adding PAP (0.1 U/mL) for 24 h. Scale bar: 100 nm.

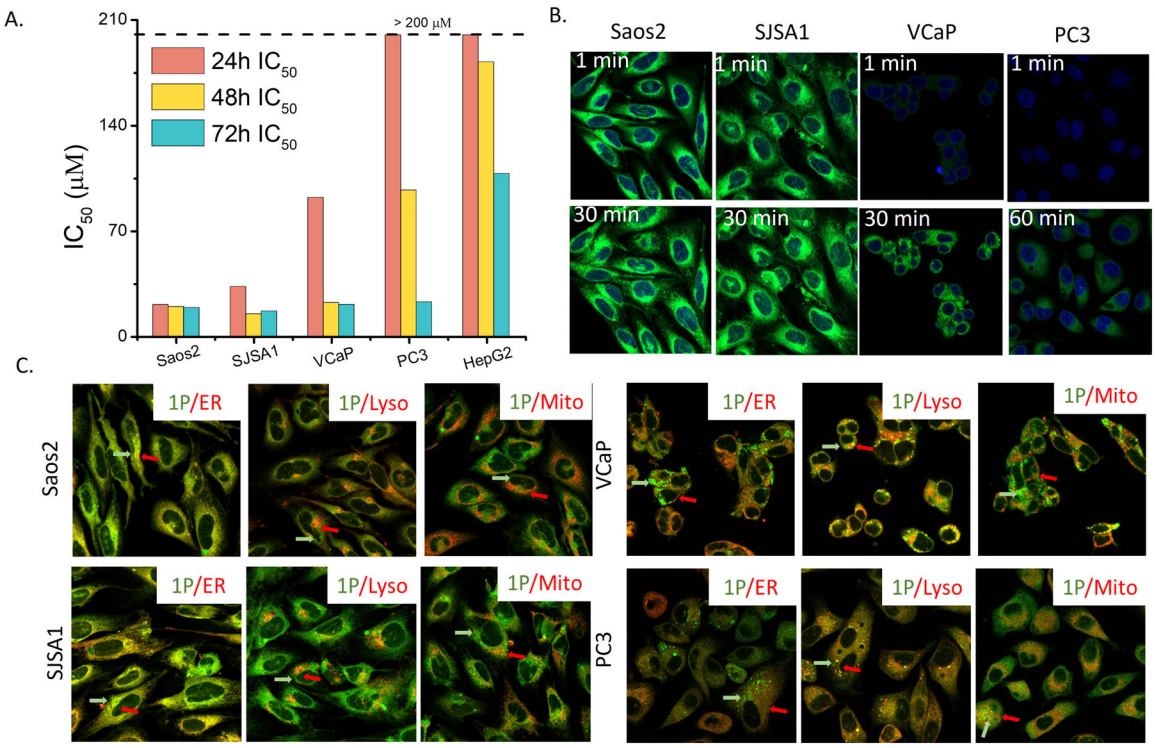

Figure 2.

(A) IC_{50} of **1P** incubated with Saos2, SJSA1, VCaP, PC3, and HepG2 cells for 24 h. (B) Instant cell entry of **1P** (100 μM). (C) Intracellular distribution of **1P** (50 μM) in Saos2, SJSA1, VCaP and PC3 after 4 h incubation. Red arrows indicate the marker, green arrow indicates **1**. Yellow indicates their colocalization.

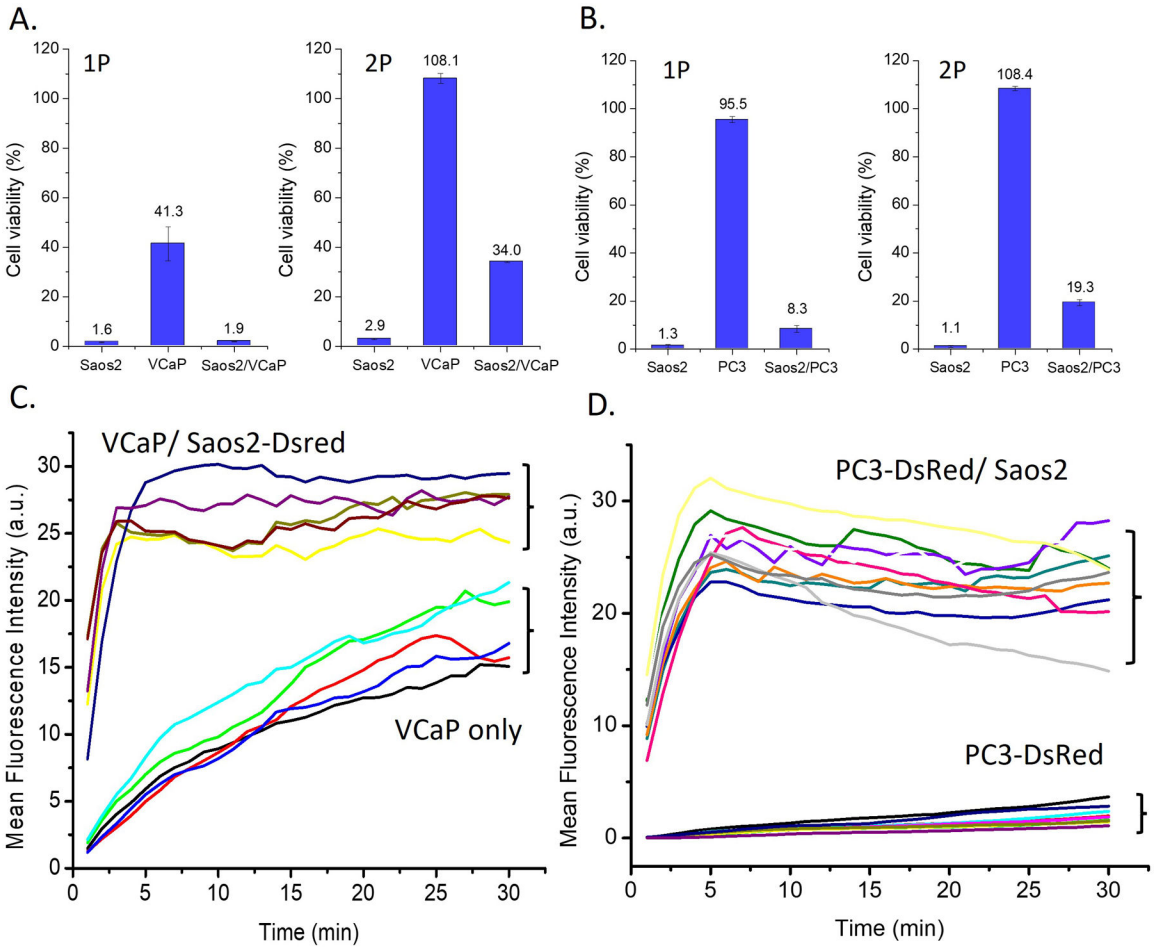

Figure 3.

Viabilities of cells treated by **1P** (100 μM) or **2P** (50 μM) in (A) Saos2, VCaP, and the coculture of Saos2 and VCaP and in (B) Saos2, PC3, and the coculture of Saos2 and PC3. The mean fluorescence intensities of **1P** (50 μM) in (C) VCaP and VCaP and the VCaP cocultured with Saos2-DsRed and (D) PC3-DsRed cells and the PC3-DsRed cocultured with Saos2 (each line representing one cell).

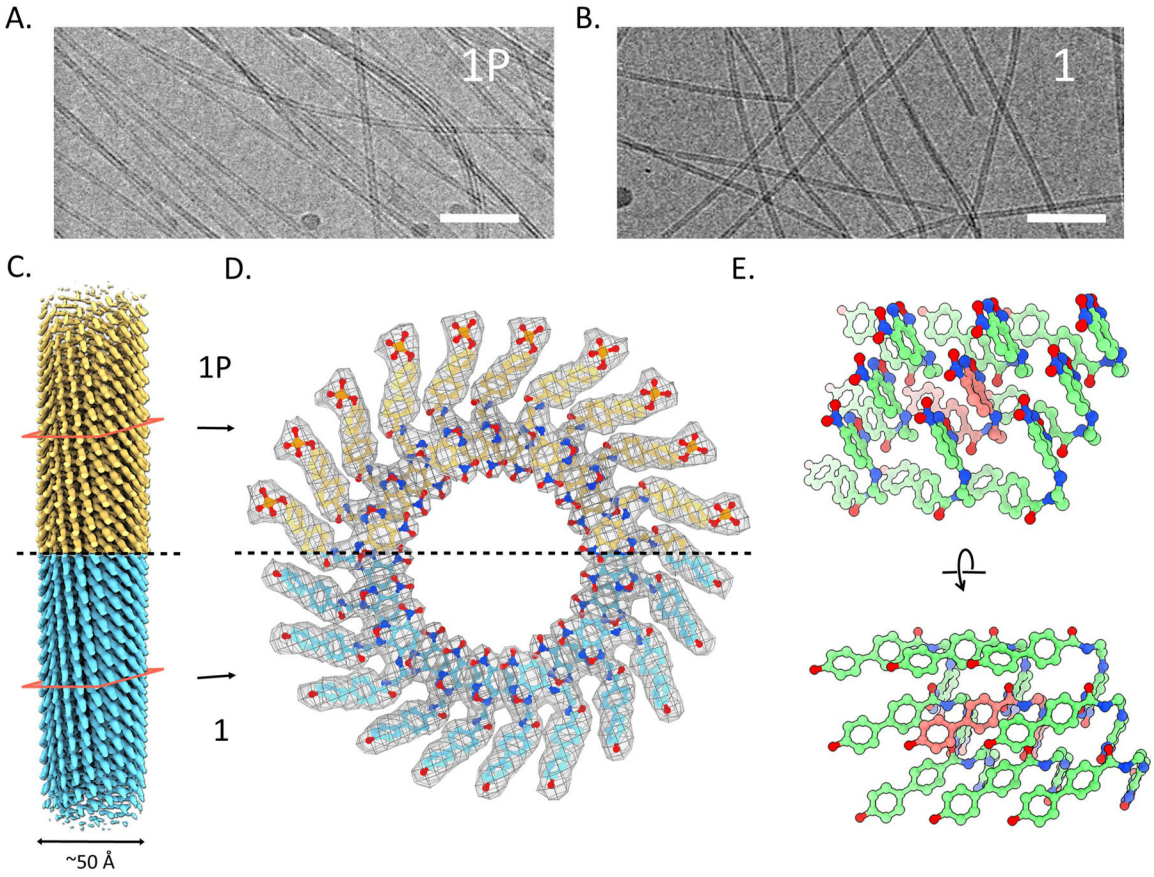

Figure 4.

A cyro-EM images of the filaments of (A) **1P** and (B) **1**. Scale bar 50 nm. (C) 3D reconstruction of tubes of **1P** and **1** from cryo-EM. (D) Top view of tubes of **1P** and **1**, phosphate of **1P** can be seen at the periphery. (E) Side view of tubes of **1**.

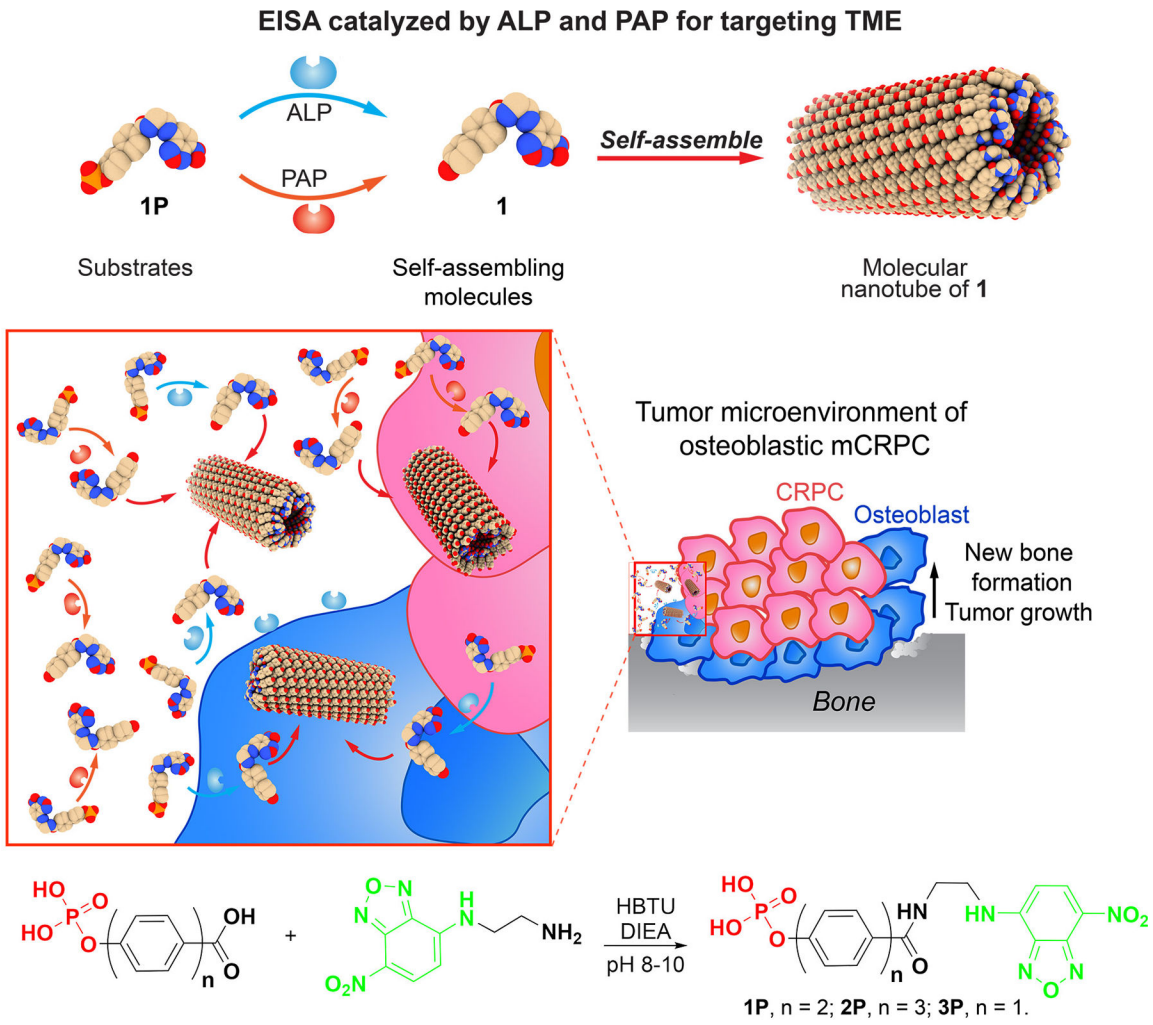

Scheme 1.

EISA for simultaneously killing mCRPC and osteoblast cells and the relevant synthesis.